

Fermi Surface Resonance and Quantum Criticality in Strongly Interacting Fermi Gases

Dmitry Miserev,^{1*} Jelena Klinovaja,¹ and Daniel Loss¹

¹*Department of Physics, University of Basel,
Klingelbergstrasse 82, CH-4056 Basel, Switzerland*

(Dated: December 2, 2020)

Fermions in a Fermi gas obey the Pauli exclusion principle restricting any two fermions from occupying the same quantum state. Strong interactions between fermions can completely change the properties of the Fermi gas. In our theoretical study we find a new exotic quantum phase in strongly interacting Fermi gases subject to a certain condition imposed on the Fermi surfaces that we call the Fermi surface resonance. The new phase is quantum critical in time and space and can be identified by the power-law dependence of the spectral density in frequency and momentum. The linear response functions are singular in the static limit and at the Kohn anomalies. We analyze the quantum critical state at finite temperatures T and finite size L of the Fermi gas and provide a qualitative L - T phase diagram. The new quantum critical phase can be experimentally found in typical semiconductor heterostructures.

I. INTRODUCTION

Physical properties of Fermi gases in a large variety of different materials have been extensively studied over the past century [1]. Properties of the non-interacting Fermi gas are entirely determined by single-particle physics and the Fermi statistics [2]. Fermions in condensed matter physics are represented by electrons or holes that interact via the Coulomb force. The Coulomb interaction between fermions can significantly change the properties of a Fermi gas. For example, a one-dimensional Fermi gas forms the strongly correlated Tomonaga-Luttinger liquid at arbitrarily weak interactions [3–5]. In higher spatial dimensions, however, weak interactions do not spoil the properties of Fermi gases but only slightly change the non-interacting characteristics. The gas of such weakly interacting fermions can be modeled by the gas of “dressed” non-interacting Landau quasiparticles. The gas of Landau quasiparticles is known as the Landau Fermi liquid (LFL) [6].

If the interaction is strong, the LFL breaks down and the ground state of the strongly interacting fermion system can dramatically change. The interaction strength is measured by the dimensionless interaction parameter r_s :

$$r_s = \frac{v_C}{E_F} \sim \frac{m e^2}{\epsilon n^{1/D}}, \quad (1)$$

where v_C is the Coulomb interaction (on average), E_F the Fermi energy, n the fermion density, m the effective mass, e the elementary charge, ϵ the dielectric constant, and D the spatial dimension. Thus, in order to drive the system into the strongly interacting regime $r_s \gg 1$, we generally need a large effective mass m , small dielectric constant ϵ and small density n . For example, the strongly interacting electron gas in near magic angle twisted bilayer graphene exhibits exotic magnetism [7], charge density order [8], and unconventional superconductivity [9], because $r_s \gg 1$ due to the low electron density and large

effective mass. The hole-doped semiconductors such as GaAs, InAs, InSb [10], or Ge [11] are also good candidates because of the large effective hole mass. The hole density n can be tuned to sufficiently small values by the electrostatic gates. Taking a two-dimensional semiconductor [10] with $\epsilon = 10$, $m = 0.2m_0$, where m_0 is the bare electron mass, and $n = 10^{11} \text{ cm}^{-2}$, we get $r_s \sim 10 \gg 1$, which corresponds to the strongly interacting regime.

The Coulomb interaction between charged fermions can be divided into two physically different parts. The first one is the classical electrostatic interaction with other electric charges via the charge density. In quantum physics there is one more type of interaction which comes from the quantum indistinguishability of two interacting fermions of the same type. This is the exchange interaction [12]. The exchange interaction can mix quasiparticles from different Fermi surfaces. In our study we show that, under certain conditions on the Fermi surfaces, the exchange interaction mixes the fermions into a new exotic phase. In this new phase the fermions form a strongly interacting quantum liquid and the LFL quasiparticle picture breaks down.

In the absence of quasiparticles there is no simple visual picture to characterize quantum processes. In order to describe quantum liquids with no quasiparticles, a quantum field description is required [13]. Excitations or quanta of the fermion fields in the LFL are long lived and they represent the Landau quasiparticles. The Heisenberg uncertainty principle obliges all physical fields to fluctuate. For example, quantum fluctuations in the LFL result in the finite lifetime of the Landau quasiparticles [14]. However, quantum fluctuations in strongly interacting quantum liquids completely destroy quasiparticles [15]. This means that all field excitations are strongly damped by the quantum fluctuations and cannot be considered as sharply defined long lived resonances. The single-particle methods in such quantum liquids are inadequate and, instead, the fermion correlations must be considered.

In this work we calculate the fermion Green function. The Green function is connected to some observables, e.g. to the spectral function and to linear response functions such as conductivity and spin susceptibility. The spectral function in the new phase contains no quasiparticle poles and instead shows universal power-law scaling with frequency and momentum. The linear response functions are singular in the static limit and at the Kohn anomalies. Strongly interacting quantum liquids with these properties are called quantum critical [16].

Quantum criticality in itinerant electron gases has been considered previously in application to cuprates [17–19]. Corresponding theoretical models are either based on the coupling of fermions to a bosonic critical order parameter [20–22], or on proximity to the Mott transition [23], or on the Sachdev-Ye-Kitaev (SYK) [24, 25] scenario of quantum criticality [26–28]. The SYK model describes flat band fermions with long range all-to-all interactions whose matrix elements are randomly distributed. In our model, we do not couple fermions to a critical order parameter, neither do we consider the Mott transition nor require random or even long-range interaction. The quantum criticality in our model emerges due to a resonant many-body exchange interaction between electrons that belong to different Fermi surfaces. This resonance, referred to as Fermi surface resonance (FSR), is the crucial feature of our model with far reaching consequences, both theoretically and experimentally, as explained in great detail in the following sections.

This work is organized as follows. In Sec. II we describe the FSR and provide an example of a realistic physical system which can be tuned to the FSR. In Sec. III we construct the effective Hamiltonian which is sensitive to the FSR. In Sec. IV we calculate the electron self-energy corresponding to the effective Hamiltonian. In Sec. V we investigate the strong coupling limit which is characterized by the emergent temporal and spatial conformal symmetry. The temporal part of the Green function is shown to obey the SYK equation, while the spatial part obeys a generalized version of it. In Sec. VI we fix the interaction strength and consider the crossover between the LFL and the quantum critical state on the L - T diagram, where T is the temperature and L the sample size. The linear response functions in the quantum critical state are calculated in Sec. VII. We find a temperature behavior of the resistance similar to the one found in strange metals. Conclusions are given in Sec. VIII. Some technical details are deferred to two appendices.

II. FERMION SURFACE RESONANCE

In our study we consider a Fermi gas with multiple non-degenerate Fermi surfaces. This can be experimentally realized in semiconductor heterostructures [29]. Semiconductor heterostructures consist of thin semiconductor layers. The contact potential between the layers confines electrons or holes within one layer. This leads to quan-

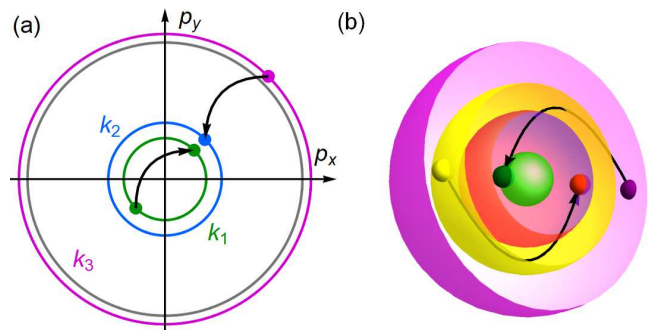


FIG. 1. Examples of the FSR. Some of the elementary resonant processes (not all of them) are shown by the arrows. (a) The simplest example of FSR can be realized in semiconductor heterostructures with two filled subbands, see Eq. (4). The spin degeneracy of the subbands is lifted by the applied magnetic field. The resonant Fermi surfaces are indicated by color. The gray Fermi surface is off resonance. (b) 3D example of the FSR. Only the resonant Fermi surfaces are shown.

tized energy subbands corresponding to different confined modes. Filling multiple subbands results in multiple Fermi surfaces, see Fig. 1. Generally, the Fermi surfaces are degenerate due to spin. The spin degeneracy can be lifted by an applied in-plane magnetic field or by spin-orbit interaction [30]. The spin-orbit interaction can be precisely tuned by electric gates [31]. We assume that $2N$, $N \geq 2$, of the non-degenerate Fermi surfaces can be tuned close to the FSR:

$$\mathcal{K} = 0, \quad (2)$$

where \mathcal{K} is a momentum mismatch between the corresponding Fermi momenta $k_a > 0$ of the involved Fermi surfaces (we assume $\hbar = 1$ throughout),

$$\mathcal{K} = k_1 + \dots + k_{N+\sigma} - k_{N+\sigma+1} - \dots - k_{2N}. \quad (3)$$

Here, $\sigma \in \{0, 1, \dots, N-1\}$. Not all Fermi surfaces are required to take part in the resonance, e.g. see Fig. 1(a). The Fermi surfaces are assumed to be spherically symmetric. This is often the case in semiconductor heterostructures because the electron and hole dispersions at small densities are nearly isotropic [32].

Equation (2) can be thought of as a radial nesting of the Fermi surfaces. Generally, nesting implies a one-dimensional character of the scattering between the nested parts of the Fermi surface. This leads to strong enhancement of such scattering which can trigger an instability. Celebrated examples of instabilities driven by nesting are the charge and spin density orders [33, 34]. The radial nesting is also known to result in strongly interacting electron states such as fractional topological insulators with a gap [35, 36]. In our study we show that the radial nesting of the Fermi surfaces given by Eq. (2) leads to a gapless quantum critical state.

In the general formulation of the problem we require all $2N$ non-degenerate Fermi surfaces participating in the

resonant $N \rightarrow N$ scattering [see Eqs. (2), (3)] to be different. However, we can soften this and only require that the N initial states belong to different Fermi surfaces, and similarly for the N final states; some of the initial states might then have the same Fermi surface index as some of the final states. In the example shown in Fig. 1(a) the FSR corresponds to the following condition:

$$2k_1 + k_2 - k_3 = 0, \quad (4)$$

where k_a , again, are the Fermi momenta of corresponding Fermi surfaces. The gray Fermi surface in Fig. 1(a) does not participate in the resonant scattering. This example corresponds to the soft formulation because the green Fermi surface contains initial and final states. The integer N in the soft formulation corresponds to the N -particle resonant scattering amplitude, e.g. $N = 2$ in Fig. 1(a).

In order to study the new quantum critical phase experimentally, one has to satisfy the single resonant condition given by Eq. (2). In addition, one has to ensure that the Fermi gas is strongly interacting, i.e. $r_s \gg 1$. We argue that semiconductor heterostructures are most promising candidates for the experimental search for such new phases. The simplest example of a semiconductor heterostructure that can host a new exotic quantum critical phase is shown in Fig. 1(a), which represents the Fermi surfaces of a two-dimensional electron gas with two occupied subbands. Even though the occupation of multiple subbands is experimentally achievable [37, 38], the experimental research of materials with multiple Fermi surfaces is still very limited which partially explains why this new phase has never been detected before. Each subband in Fig. 1(a) is split by an external magnetic field. Changing the electron density and fine tuning by the magnetic Zeeman splitting we can set the system to the FSR given by Eq. (4). The given example corresponds to the $N = 2$ particle resonant scattering amplitude within the soft formulation of the FSR because the green Fermi surface contains both initial and final states. The FSR results in the strong mixing of three colored bands in Fig. 1(a) which destroys quasiparticles in the vicinity of the colored Fermi surfaces. The quasiparticles in the vicinity of the off-resonant gray Fermi surface survive. The new phase in this example has separate Fermi-liquid and non-Fermi-liquid components. The latter is established at the resonance given by Eq. (4) and can be experimentally identified from the power-law frequency and momentum dependence of the spectral function and the singular linear response functions in the static limit and at the Kohn anomalies (see below).

In what follows we consider the general case of $D > 1$ spatial dimensions. A $D = 3$ example of the strong version of the FSR with $2N = 4$ different Fermi surfaces is shown in Fig. 1(b).

III. EFFECTIVE HAMILTONIAN

Now we proceed to the general case of the FSR. Here we assume that all $2N$ fields participating in the resonance are different, see Eq. (2). All the results that we obtain in this paper also apply to the soft version of the FSR where some initial states might have the same Fermi surface index as some final states, see Fig. 1(a). The FSR results in a dramatic change of the ground state because it favors resonant many-body exchange scattering. The FSR is applied to $2N$ different non-degenerate Fermi surfaces, so we consider an $N \rightarrow N$ scattering amplitude which is multilinear with respect to each fermion field. As the FSR condition says nothing about initial and final states, we have to sum over all possible choices of N initial and N final states out of overall $2N$ fields corresponding to the $2N$ Fermi surfaces, yielding the following effective Hamiltonian:

$$V(R) = \sum_{\{j\}} \lambda_j \Psi_{j_1}^\dagger(R) \dots \Psi_{j_N}^\dagger(R) \Psi_{j_{N+1}}(R) \dots \Psi_{j_{2N}}(R), \quad (5)$$

where $R = (t, \mathbf{r})$, \mathbf{r} is a D -dimensional position vector, t the time, j a permutation of indices $\{1, \dots, 2N\}$, $\Psi_a(R)$ the fermion field operator corresponding to the a^{th} Fermi surface, and λ_j are the coupling constants. We sum over all non-equivalent permutations corresponding to $C_{2N}^N = (2N)!/(N!)^2$ different choices of initial and final states. For conjugate terms the corresponding λ_j is a complex conjugate in order to ensure hermiticity of $V(R)$. The effective Hamiltonian $V(R)$ is of exchange form as it mixes together all $2N$ fermion fields corresponding to the $2N$ Fermi surfaces participating in the resonance. Similar in spirit is the effective Hamiltonian approach widely used in condensed matter physics, in particular, in the weakly coupled wire approach where N -electron effective inter-wire interactions are constructed [39–41].

In case of the soft formulation, the effective Hamiltonian has the same form as Eq. (5). The only difference is that the terms containing the square of field operators vanish due to the Fermi statistics. This is consistent with our requirement that all N initial states as well as all N final states belong to N different Fermi surfaces.

The effective Hamiltonian, see Eq. (5), can be constructed using perturbation theory with respect to the two-particle Coulomb interaction, v_C . The first contribution to $V(R)$ comes from the tree diagrams in the $(N - 1)^{\text{th}}$ order in v_C :

$$V(R) \propto \Lambda = \frac{v_C^{N-1}}{E_F^{N-2}} = E_F r_s^{N-1}, \quad (6)$$

where Λ is the characteristic energy scale of $V(R)$, E_F the Fermi energy, and r_s the interaction parameter given by Eq. (1). The power of v_C corresponds to the order of perturbation theory, the power of $1/E_F$ corresponds to the number of fermion propagators in the tree diagrams. Notice that the strongly interacting regime $r_s \gg 1$ also corresponds to $\Lambda \gg E_F$. Each of the tree diagrams can

be envisioned as a sequence of $N - 1$ Coulomb exchange scattering events. As all $2N$ fermions are different, the momentum transfers during the exchange are all in order of the average Fermi momentum k_F . We are interested in the long range correlations at relative distance $r \gg 1/k_F$. For such long range correlations the $N \rightarrow N$ scattering that occurs on the scale of the Fermi wavelength $\sim 1/k_F$ is effectively local, justifying the locality of $V(R)$. All the matrix elements that appear in the tree diagrams for $V(R)$ are hidden in the coupling constants λ_j . Higher order diagrams for $V(R)$ only renormalize the coupling constants λ_j . Due to symmetries of specific Hamiltonians some of the coupling constants λ_j might be equal to zero. However, this fact is not important for the further analysis if there are at least some non-zero λ_j .

We argue that $V(R)$ is the most important scattering amplitude close to the FSR, see Eq. (2). All other terms in the many-body scattering amplitudes are either insensitive to the FSR or contain rapidly oscillating terms on the scale of Fermi wavelength. Here we work within the assumption that at arbitrary filling electrons or holes in semiconductors form the LFL. This means that the interaction which is not sensitive to the FSR cannot significantly change the physics. Interactions that contain oscillating terms can be averaged to zero on large scales $r \gg 1/k_F$. This allows one to include such interactions as irrelevant corrections renormalizing the LFL parameters.

The effective Hamiltonian $V(R)$ is very sensitive to the FSR condition given by Eq. (2). Further we show that exactly at the FSR it results in the emergent long-range order and the destruction of the quasiparticle picture in the infrared limit.

IV. DIMENSIONAL REDUCTION

In this section we calculate the fermion Green function dressed by the effective interaction $V(R)$, see Eq. (5). Here we show that a strong interaction $V(R)$ completely destroys quasiparticles close to the Fermi surfaces. The notion of Fermi surfaces is still important though because they define the sector of quantum states that are most affected by the interaction $V(R)$. Such Fermi surfaces without quasiparticles are known as critical Fermi surfaces [27].

Far away from the Fermi surfaces the resonant scattering is destroyed and thus we expect the LFL in the ultraviolet limit even when the FSR condition Eq. (2) is satisfied. Thus, for large $\omega_a \sim E_F$ and $\delta p_a = p_a - k_a \sim k_a$ the Green function restores the quasiparticle poles:

$$G_a^{(0)}(\omega_a, \delta p_a) = \frac{Z_a}{\omega_a - v_a \delta p_a}, \quad (7)$$

where E_F is the Fermi energy, the index $a \in \{1, \dots, 2N\}$ enumerates the Fermi surfaces, ω_a and p_a are the frequency and the momentum, k_a is the Fermi momentum of the a^{th} Fermi surface, v_a is the Fermi velocity which is renormalized by irrelevant interactions, and $1 > Z_a > 0$

is the quasiparticle residue away from the Fermi surface. We allow the frequency ω_a to be complex. For example, imaginary frequencies correspond to the Matsubara formalism, while $\omega_a \rightarrow \omega_a + i0$ yields the retarded Green function. In this section we calculate the Matsubara Green function at zero temperature. Other Green functions can be obtained via the analytical continuation through the spectral representation [42]:

$$G_a(\omega_a, \delta p_a) = \int_{-\infty}^{\infty} \frac{dz}{\pi} \frac{\mathcal{A}_a(z, \delta p_a)}{\omega_a - z}, \quad (8)$$

where $\mathcal{A}_a(\omega_a, \delta p_a) = -\text{Im}[G_a(\omega_a + i0, \delta p_a)] > 0$ is the positively defined spectral function, and Im stands for the imaginary part.

Close to the FSR, see Eqs. (2) and (3), the resonant many-body exchange scattering described by the effective Hamiltonian $V(R)$, see Eq. (5), becomes important in the infrared limit. We include it via the self-energy $\Sigma_a(i\omega_a, \delta p_a)$:

$$G_a(i\omega_a, \delta p_a) = \frac{1}{G_a^{(0)}(i\omega_a, \delta p_a)^{-1} - \Sigma_a(i\omega_a, \delta p_a)}, \quad (9)$$

where $G_a^{(0)}(i\omega_a, \delta p_a)$ is given by Eq. (7) and contains the contributions from the irrelevant interactions, ω_a is the fermionic Matsubara frequency. We assume here that there is no Pomeranchuk instability [43] even in the strongly interacting regime, so the spherical symmetry of the Fermi surfaces is exact. In this case the fermion Green function $G_a(\tau, \mathbf{r})$ in the imaginary time-coordinate representation depends only on the absolute value $r = |\mathbf{r}|$. This allows for the effective one-dimensional representation of the Green function:

$$G_a(\tau, r) = \sum_{\mathbf{p}_a} e^{i\mathbf{p}_a \cdot \mathbf{r}} G_a(\tau, \delta p_a) = \int_{-k_a}^{\infty} \frac{d\delta p_a}{2\pi} p_a^{D-1} J(rp_a) G_a(\tau, \delta p_a), \quad (10)$$

$$\sum_{\mathbf{p}_a} \equiv \int \frac{d\mathbf{p}_a}{(2\pi)^D} = \int \frac{d\Omega_D}{(2\pi)^{D-1}} \frac{d\delta p_a}{2\pi} p_a^{D-1}, \quad (11)$$

$$J(z) = \int \frac{d\Omega_D e^{iz \cos \theta}}{(2\pi)^{D-1}} \rightarrow \frac{2 \cos(|z| - \frac{\pi}{2} \frac{D-1}{2})}{(2\pi|z|)^{\frac{D-1}{2}}}, \quad (12)$$

where $\delta p_a = p_a - k_a$, k_a is the Fermi momentum of the a^{th} Fermi surface, $d\Omega_D$ is the volume element of the D -dimensional solid angle. In Eq. (12) we also provide the asymptotic behavior of $J(z)$ for large argument $|z| \gg 1$. We use this to derive the long distance form of the Green function:

$$G_a(\tau, r) \rightarrow \left(\frac{k_a}{2\pi r} \right)^{\frac{D-1}{2}} \times \left[i^{-\frac{D-1}{2}} e^{ik_a r} \mathcal{G}_a(\tau, r) + i^{\frac{D-1}{2}} e^{-ik_a r} \mathcal{G}_a(\tau, -r) \right], \quad (13)$$

$$\mathcal{G}_a(\tau, x) = \int_{-\infty}^{\infty} \frac{d\delta p_a}{2\pi} e^{ix\delta p_a} G_a(\tau, \delta p_a), \quad (14)$$

where $r \gg 1/k_a$, and the integral over δp_a is extended to the interval $(-\infty, \infty)$ with negligible error. Here, $\mathcal{G}_a(\tau, x)$ represents a one-dimensional Fourier transform, $x \in (-\infty, \infty)$. Thus, one can consider Eqs. (13)–(14) as the dimensional reduction from D spatial dimensions to a single spatial dimension with coordinate x which is conjugate to the momentum δp_a .

In order to calculate the effectively one-dimensional Green function $\mathcal{G}_a(\tau, x)$, see Eq. (14), we have to find the electron self-energy due to the interaction Hamiltonian $V(R)$, see Eq. (5). The Feynman diagram for the exact self-energy for $N = 2$ is presented in Fig. 2(a) and corresponds to the example shown in Fig. 1(b). Feynman diagrams for general N can be drawn in a similar fashion. The problem here is the renormalization of the interaction vertex, see full black square in Fig. 2(a). In this section we omit the interaction vertex renormalization and instead consider the simpler diagram in Fig. 2(b). Such an approximation is called the self-consistent Born approximation (SCBA). The diagrams of the form in Fig. 2(b) are also known as “melon” diagrams that appear in various matrix and tensor field theories [44].

We calculate the SCBA self-energy $\Sigma_1(\tau, \delta p_1)$, see Fig. 2(b), in the imaginary time-coordinate representation:

$$\Sigma_1(\tau, r) = (-1)^{N-1} \sum_{\{\eta\}} |\lambda_\eta|^2 \prod_{a=2}^{2N} G_a(\eta_a \tau, r), \quad (15)$$

where λ_η are the bare interaction coupling constants, see Eq. (5). We consider the self-energy corresponding to the electrons near the 1st Fermi surface, the result is similar for other Fermi surface indices. Each $\eta = (\eta_2, \dots, \eta_{2N})$, $\eta_b = \pm 1$, corresponds to one of the choices to draw arrows on the Feynman diagram, one of such choices is shown in Fig. 2(b). The charge conservation imposes the following constraint:

$$\sum_{b=2}^{2N} \eta_b = 1. \quad (16)$$

This gives overall $C_{2N-1}^N = (2N-1)!/(N!(N-1)!)$ terms in the sum over η . The long-distance asymptotics of the self-energy takes the form of Eq. (13):

$$\begin{aligned} \Sigma_1(\tau, r) &\rightarrow \left(\frac{k_1}{2\pi r}\right)^{\frac{D-1}{2}} \\ &\times \left[i^{-\frac{D-1}{2}} e^{ik_1 r} \mathcal{S}_1(\tau, r) + i^{\frac{D-1}{2}} e^{-ik_1 r} \mathcal{S}_1(\tau, -r) \right], \quad (17) \end{aligned}$$

$$\mathcal{S}_1(\tau, x) = \int_{-\infty}^{\infty} \frac{d\delta p_1}{2\pi} e^{ix\delta p_1} \Sigma_1(\tau, \delta p_1), \quad (18)$$

where $\mathcal{S}_1(\tau, x)$ is a one-dimensional self-energy. In order to find $\mathcal{S}_1(\tau, x)$, we substitute the asymptotic expansion

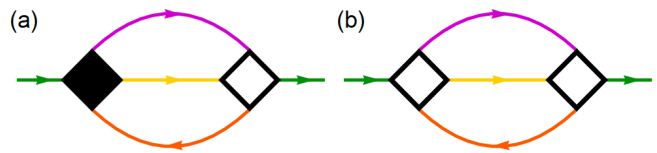


FIG. 2. Electron self-energy. (a) Feynman diagram for the exact self-energy for the case $N = 2$. Solid lines correspond to the exact Green functions, see Eq. (9). The Fermi surface index $a \in \{1, 2, 3, 4\}$ is indicated by color and corresponds to the example given in Fig. 1(b). The black (white) square corresponds to the exact (bare) interaction vertex. There are two more contributions to the self-energy that differ by the arrow directions. The Feynman diagrams for general N can be drawn similarly. (b) The SCBA. The interaction vertex correction is neglected which is shown by two bare vertices (white squares).

Eq. (13) of the Green functions in Eq. (15) and compare with Eq. (17):

$$\mathcal{S}_1(\tau, x) = (-1)^{N-1} c_1 \sum_{\{\eta\}} |\lambda_\eta|^2 \prod_{a=2}^{2N} \mathcal{G}_a(\eta_a \tau, s_a x) \mathcal{D}(x), \quad (19)$$

$$\mathcal{D}(x) = \frac{e^{-i\mathcal{K}x}}{|x|^{2\nu}} i^{\sigma(D-1)\text{sgn}(x)}, \quad \nu = \frac{1}{2}(N-1)(D-1), \quad (20)$$

where $s_a = -1$ ($s_a = +1$) for $a \in \{2, \dots, N + \sigma\}$ ($a \in \{N + \sigma + 1, \dots, 2N\}$), $|\mathcal{K}| \ll k_a$ and σ are defined in Eq. (2) and c_1 is the following constant:

$$c_1 = \left(\frac{k_F}{k_1}\right)^{D-1} \left(\frac{k_F}{2\pi}\right)^{2\nu}, \quad (k_F)^{2N} \equiv k_1 \cdot \dots \cdot k_{2N}, \quad (21)$$

where k_F is the average Fermi momentum. In Eq. (19) we only retained slowly varying terms because we are interested in the long distance correlations. Note that $1/\mathcal{K}$ is the only length scale that survived the dimensional reduction. The fluctuations at $|x| \gg 1/|\mathcal{K}|$ are not important due to the oscillating exponential in Eq. (20), and thus $1/|\mathcal{K}|$ defines the finite range of the interaction. At $\mathcal{K} = 0$ there are no internal length scales that enter Eq. (19) which results in the emergent long range order.

V. STRONG COUPLING LIMIT

In this section we consider the strong coupling regime, when the Green function close to the Fermi surfaces, see Eq. (9), is entirely defined by its self-energy:

$$G_a(i\omega_a, \delta p_a) \approx -\frac{1}{\Sigma_a(i\omega_a, \delta p_a)}. \quad (22)$$

This approximation breaks down far away from the Fermi surfaces where the many-body scattering is off-resonant. In other words, the LFL is restored in the ultraviolet limit far away from the Fermi surface. Only the quantum states close to the Fermi surface are strongly affected

by the interaction. These quantum states represent the infrared sector of the problem.

In the (τ, x) representation Eq. (22) takes the integral form:

$$\delta(\tau)\delta(x) = - \int d\tau' dx' \mathcal{G}_a(\tau - \tau', x - x') \mathcal{S}_a(\tau', x'), \quad (23)$$

where $\mathcal{G}_a(\tau, x)$ and $\mathcal{S}_a(\tau, x)$ are defined in Eqs. (14) and (18), respectively. Substituting Eq. (19) into Eq. (23) results in the integral Dyson equation for the Green function calculated within the SCBA and in the strong coupling limit:

$$\begin{aligned} \delta(\tau)\delta(x) &= (-1)^N c_1 \int d\tau' dx' \mathcal{G}_1(\tau - \tau', x - x') \\ &\times \sum_{\{\eta\}} |\lambda_\eta|^2 \prod_{a=2}^{2N} \mathcal{G}_a(\eta_a \tau', s_a x') \mathcal{D}(x'). \end{aligned} \quad (24)$$

At the FSR the effective interaction $\mathcal{D}(x)$ is quasi-long-range, i.e. it looks the same at all scales, see Eq. (20) at $\mathcal{K} = 0$. In contrast to Eqs. (9) and (15) for the total Green function and the self-energy, which contain the information about the physical scales such as the Fermi momenta k_a and corresponding band splittings, Eq. (24) is free from any physical energy or length scale. This observation suggests that the Green functions in Eq. (24) are also universal scaling functions. As all $2N$ Green functions occur in the product in Eq. (24), they are equivalent, and, thus, we expect the same critical exponents for all of them regardless of the index a . A simple dimensional analysis of Eq. (24) yields:

$$\mathcal{G}_a(\tau, x) \propto \frac{1}{|\tau|^{2h}} \frac{1}{|x|^{2l}}, \quad h = \frac{1}{2N}, \quad l = \frac{1-\nu}{2N}, \quad (25)$$

where ν is given by Eq. (20). The time and coordinate scalings of the Green function are different due to the effective interaction $\mathcal{D}(x)$. This naturally suggests the separation of temporal and spatial dynamics:

$$\mathcal{G}_a(\tau, x) = C_a g(\tau) \gamma(x), \quad (26)$$

where C_a is some constant that might be different for different a . This ansatz is different from the truly one-dimensional case $D = 1$ in which the temporal and spatial scalings are the same and the separation argument does not apply for $D = 1$. Instead, left and right linear combinations of time and coordinate must be used for $D = 1$. Thus, our current analysis of Eq. (24) is only applicable for $D > 1$ where the effective interaction $\mathcal{D}(x)$ breaks the equivalence between time and coordinate. The Dyson Eq. (24) then separates into a time and a coordinate equation:

$$\delta(\tau) = (-1)^N \int d\tau' g(\tau - \tau') g(-\tau')^{N-1} g(\tau')^N, \quad (27)$$

$$\delta(x) = \int dx' \gamma(x - x') \gamma(-x')^{N+\sigma-1} \gamma(x')^{N-\sigma} \mathcal{D}(x'). \quad (28)$$

As only the product of $g(\tau)$ and $\gamma(x)$ is important, see Eq. (26), we have an additional symmetry under the

transformation $g(\tau) \rightarrow Cg(\tau)$ and $\gamma(x) \rightarrow \gamma(x)/C$ for any complex $C \neq 0$. The coefficients C_a satisfy the following algebraic equation:

$$c_1 \lambda^2 \prod_{a=1}^{2N} C_a = 1, \quad \lambda = \sqrt{\sum_{\{\eta\}} |\lambda_\eta|^2}. \quad (29)$$

Equation (29) will be different if we consider the Dyson equation Eq. (23) for some other Fermi surface index $a \neq 1$. This is due to the non-universal coefficient $c_1 \propto k_1^{1-D}$, see Eq. (21), which is in general replaced by $c_a \propto k_a^{1-D}$. At the same time the product of all coefficients C_a in Eq. (29) is independent of the Fermi surface index. This apparent conflict arises due to inadequacy of the long distance expansion, Eq. (13), at small distances $r \lesssim 1/k_F$, k_F is an average Fermi momentum. Indeed, the right hand side of Eq. (24) has to diverge at $x = 0$ which corresponds to the ultraviolet divergence of the propagators $\mathcal{G}_a(\tau, x)$ at $x = 0$, see Eq. (25). On the other hand, such a divergence at small $r \lesssim 1/k_F$ is regularized (and thus absent) in the exact Green function $G_a(\tau, r)$. In other words, the long-distance infrared limit that we take here does not allow us to define the exact numerical prefactor in Eq. (24) as it depends on the ultraviolet regularization. At the same time, the scale-independent limit of the Dyson Eq. (24) at $\mathcal{K} = 0$ implies that c_1 has to be replaced by a universal coefficient c which we estimate via dimensional analysis:

$$c_1 \rightarrow c \sim \left(\frac{k_F}{2\pi} \right)^{2\nu}. \quad (30)$$

We can choose all coefficients C_a positive, i.e. $C_a > 0$. Non-trivial phases can come from solutions for $g(\tau)$ and $\gamma(x)$ which we consider later. All coefficients $C_a > 0$ are combined in the single product in Eq. (29) with c_1 replaced by c , see Eq. (30), so it is not possible to determine them separately without connecting the infrared interaction-dominated limit with the ultraviolet limit far away from the Fermi surfaces which is given by the LFL. From Eq. (29) we conclude that the coefficients C_a scale with the interaction strength as $C_a \propto \lambda^{-1/N}$. This corresponds to the following self-energy scaling:

$$\Sigma_a \propto \lambda^{1/N}. \quad (31)$$

This scaling justifies the strongly interacting limit $\lambda \rightarrow \infty$ at which the self-energy correction is dominant over the single-particle spectral part. Apart from the considered interaction scaling, the coefficients C_a play no role in the infrared physics that we study here, so we can concentrate on the universal functions $g(\tau)$ and $\gamma(x)$.

We observe here that Eq. (27) is the Dyson equation for the generalized SYK model, referred to as q -SYK model [24, 25], with $q = 2N$ in our case. The SYK model describes $(0+1)$ -dimensional strongly correlated fermions with all-to-all interactions whose matrix elements are randomly distributed. Quite remarkably, the temporal dynamics for our $(D+1)$ -dimensional system

without having any randomness in our model and for short-range interactions given by the Hamiltonian $V(R)$, see Eq. (5), maps exactly onto the q -SYK model with $q = 2N$. The SYK model is the central example of the AdS/CFT correspondence [45] and plays an important role in understanding the nature of strange metals [26–28]. In contrast to Eq. (27), Eq. (28) contains the effective interaction $\mathcal{D}(x)$ which can be interpreted as a propagator of an emergent complex boson. This emergent boson is merely a result of the dimensional reduction. Its propagator $\mathcal{D}(x)$ contains the momentum mismatch \mathcal{K} (which is zero at the FSR) and the geometric factors coming from the s -wave expansion of the fermion propagators, see Eqs. (13) and (20).

The Matsubara Green function $G_a(\tau, r)$, see Eq. (13), has to be real-valued which is evident from the spectral representation, see Eq. (8). This is equivalent to the following constraint:

$$\mathcal{G}_a^*(\tau, r) = \mathcal{G}_a(\tau, -r), \quad (32)$$

where $\mathcal{G}_a(\tau, r)$ is defined in Eq. (14). Together with the separation of variables, see Eq. (26), this results in the following conditions on the universal functions $g(\tau)$ and $\gamma(x)$:

$$g^*(\tau) = g(\tau), \quad \gamma^*(-x) = \gamma(x). \quad (33)$$

In other words, $g(\tau)$ and $\gamma(\delta p)$ have to be real-valued functions. Following Refs. [25, 26], we find the universal functions $g(\tau)$ and $\gamma(x)$:

$$g(\tau) \propto \frac{\text{sgn}(\tau)}{|\tau|^{2h}}, \quad (34)$$

$$\gamma(x) \propto \frac{1}{|x|^{2l}}, \quad (35)$$

where we used the symmetry of Eq. (33).

Equation (27) can be easily extended to the case of finite temperature T due to the emergent conformal symmetry, for details see Refs. [25, 26]:

$$g_T(\tau) \propto \text{sgn}(\tau) \left| \frac{\pi T}{\sin(\pi T \tau)} \right|^{2h}, \quad (36)$$

where $\tau \in (-1/T, 1/T)$ is the imaginary time, with the Boltzmann constant set to $k_B = 1$. Using Eqs. (13), (26), (34), and (35), we find explicitly the long time and long distance asymptotics of the finite temperature Matsubara Green function:

$$G_a(\tau, r) \propto \text{sgn}(\tau) \left| \frac{\pi T}{\sin(\pi T \tau)} \right|^{2h} \frac{\cos(k_a r - \frac{\pi}{2} \frac{D-1}{2})}{r^{(D+1)h}}, \quad (37)$$

where $h = 1/(2N)$ is the temporal scaling dimension. The corresponding Fourier transform $G_a(i\omega_a, \delta p_a)$ becomes:

$$G_a(i\omega_a, \delta p_a) = -\frac{i}{T} \left| \frac{T}{\Lambda} \right|^{2h} \left| \frac{k_a}{\delta p_a} \right|^{1-2l} \frac{\Gamma\left(h + \frac{\omega_a}{2\pi T}\right)}{\Gamma\left(1 - h + \frac{\omega_a}{2\pi T}\right)}, \quad (38)$$

where ω_a is the discrete Matsubara frequency, k_a the Fermi momentum corresponding to the a^{th} Fermi surface. Here we restored the physical dimensions using Eqs. (6), (31). The unknown numerical factors are hidden in the phenomenological ultraviolet scale Λ that defines the interaction strength, see Eq. (6).

Analytically continuing the Matsubara Green function Eq. (38) to real frequencies, we find the retarded Green function:

$$G_a^R(\omega_a, \delta p_a) = -\frac{i}{T} \left| \frac{T}{\Lambda} \right|^{2h} \left| \frac{k_a}{\delta p_a} \right|^{1-2l} \frac{\Gamma\left(h - \frac{i\omega_a}{2\pi T}\right)}{\Gamma\left(1 - h - \frac{i\omega_a}{2\pi T}\right)}, \quad (39)$$

where ω_a is a real frequency. The advanced Green function is complex conjugate to the retarded one. In the limit of large frequency $\omega \gg T$ we restore the power-law frequency scaling $G_a(\omega_a, \delta p_a) \propto |\omega_a|^{2h-1}$, where $2h-1 < 0$ signaling the singularity at $\omega \rightarrow 0$. At finite temperature T this singularity is cut as $G_a(\omega_a = 0, \delta p_a) \propto T^{2h-1}$, see Eqs. (38) and (39).

As we know the exact retarded Green function, we can calculate the fermion spectral density:

$$\begin{aligned} \mathcal{A}_a(\omega_a, \delta p_a) &= -\frac{1}{\pi} \text{Im} [G_a^R(\omega_a, \delta p_a)] = \frac{\sin(\pi h)}{\pi^2 T} \\ &\times \left| \frac{T}{\Lambda} \right|^{2h} \left| \frac{k_a}{\delta p_a} \right|^{1-2l} \cosh\left(\frac{\omega_a}{2T}\right) \left| \Gamma\left(h + \frac{i\omega_a}{2\pi T}\right) \right|^2. \end{aligned} \quad (40)$$

The temperature and frequency dependence of the spectral density correspond to the q -SYK, $q = 2N$, model, see Ref. [26]. The electron spectral function, see Eq. (40), does not contain any sharply defined quasiparticle peaks. Instead, there is the power law scaling in the momentum δp_a and frequency $\omega_a \gg T$. At low frequency $\omega_a \ll T$, the spectral density is a power-law function of temperature. Thus, measuring the momentum, frequency, and temperature scaling of the spectral density close to the Fermi surface allows one to identify experimentally the scaling dimensions h and l that determine the quantum critical point.

VI. EXACTNESS OF SCBA AND STABILITY OF THE QUANTUM CRITICAL POINT

In order to calculate the electron self-energy, we used the SCBA, i.e. we neglected the interaction vertex corrections, see Fig. 2. Here we aim to show that the SCBA is exact in the strong coupling limit. For this we investigate the symmetries of the Dyson Eqs. (27) and (28). It turns out that both equations are invariant under time and coordinate reparametrizations which constitutes the two-dimensional conformal symmetry. This means that if $g(\tau, \tau')$ [$\gamma(x, x')$] are solutions of the Dyson Eq. (27) [Eq. (28)], then the following functions $\tilde{g}(t_1, t_2)$ [$\tilde{\gamma}(\xi_1, \xi_2)$] are also solutions of the corresponding Dyson equations:

$$\tau = f_1(t), \quad x = f_2(\xi), \quad (41)$$

$$\tilde{g}(t_1, t_2) = |f'_1(t_1)f'_1(t_2)|^h g(f_1(t_1), f_1(t_2)), \quad (42)$$

$$\tilde{\gamma}(\xi_1, \xi_2) = |f'_2(\xi_1)f'_2(\xi_2)|^l \gamma(f_2(\xi_1), f_2(\xi_2)), \quad (43)$$

where $f_{1,2}(z)$ is a real-valued monotonic function, with $f'_{1,2}(z)$ being its derivative with respect to z . In contrast to the SYK Dyson Eq. (27), the spatial Dyson Eq. (28) contains the function $\mathcal{D}(x)$ which transforms as a propagator of an emergent boson field with the scaling dimension ν :

$$\tilde{\mathcal{D}}(\xi_1, \xi_2) = |f'_2(\xi_1)f'_2(\xi_2)|^\nu \mathcal{D}(f_2(\xi_1), f_2(\xi_2)). \quad (44)$$

The conformal symmetry of both temporal and spatial Dyson Eqs. (27) and (28) is signaling an interaction fixed point in the renormalization group sense. In other words, our initial ansatz that the interaction vertex is not renormalized in the infrared limit turned out to be correct in the strong coupling limit due to the emergent conformal symmetry.

So far, we have solved exactly the problem of a strongly interacting electron gas that is tuned to the FSR. However, we neglected the single-particle spectral part compared to the self-energy, see Eq. (22). The strongly interacting limit is justified if $|\Sigma_a(i\omega_a, \delta p_a)| \gg \max\{\omega_a, v_a \delta p_a\}$, see Eq. (9), where v_a is the Fermi velocity at the a^{th} Fermi surface. Here we consider the case of finite temperature T and finite size L of the system. In this case the infrared and long distance limits correspond to $\omega_a \sim T$ and $\delta p_a \sim 1/L$. Using Eqs. (22) and (38), we can estimate the self-energy at the smallest frequencies and momenta:

$$\Sigma_a(i\omega_a \sim iT, \delta p_a \sim 1/L) \propto \Lambda^{2h} T^{1-2h} (k_a L)^{2l-1}. \quad (45)$$

Therefore, the strong coupling limit corresponds to the following constraint:

$$\Lambda^{2h} T^{1-2h} (k_F L)^{2l-1} \gg \max\left\{T, \frac{v_F}{L}\right\}, \quad (46)$$

where we introduced the average Fermi momentum k_F and average Fermi velocity v_F . This condition can be represented in simpler form:

$$\frac{r_s^{N-1}}{(k_F L)^{\frac{1-2l}{2h}}} \gg \frac{T}{E_F} \gg \frac{1}{r_s} (k_F L)^{-\frac{2l}{1-2h}}, \quad (47)$$

where we used Eq. (6) to express everything in terms of $r_s \gg 1$. Here it is important that $1 - 2l > 0$ for any $N \geq 2$, $D > 1$, see Eq. (25). This results in an upper bound L^* for the system size L :

$$L \ll L^* = \frac{1}{k_F} r_s^{\frac{1-2h}{1-2h-2l}}. \quad (48)$$

Thus, the quantum critical point corresponding to $\mathcal{K} = 0$ is stable only for finite size $L \ll L^*$ and in the temperature range given by Eq. (47), see Fig. 3.

In the dimensional reduction we rely on the rotational symmetry of the Fermi surfaces. However, main conclusions of our paper will still be true in case of small asymmetry of the Fermi surfaces. Let the Fermi momentum

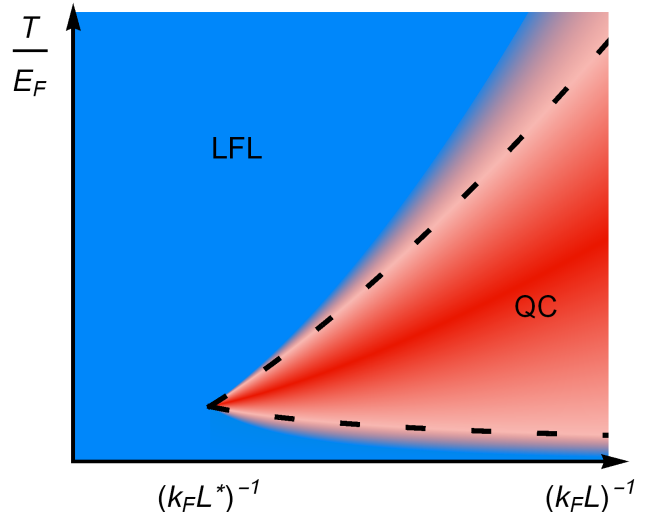


FIG. 3. The L - T phase diagram illustrating the crossover between the LFL (blue) and quantum critical (QC) state (red). The dashed lines correspond to upper and lower bounds in Eq. (47). The upper bound for the wire length L^* corresponds to Eq. (48).

of the a^{th} Fermi surface range from $k_a - \Delta k_a$ to $k_a + \Delta k_a$, where $\Delta k_a \ll k_a$. Then in addition to Eq. (47) the temperature must also satisfy $T \gg v_a \Delta k_a$. Here, v_a is the Fermi velocity of the a^{th} Fermi surface, so that the Fermi surface asymmetry is smoothed out by thermal effects. Comparing with Eq. (47) this gives an upper bound for Δk_a :

$$\frac{v_a \Delta k_a}{E_F} \ll \frac{r_s^{N-1}}{(k_F L)^{\frac{1-2l}{2h}}}. \quad (49)$$

VII. LINEAR RESPONSE FUNCTIONS

In this section we consider the linear response functions that can also be used for experimental identification [46] of the predicted quantum critical state. In case of non-degenerate Fermi surfaces the linear response functions are represented by the following charge susceptibilities that we calculate within the Matsubara technique:

$$\chi_{ab}(\tau, r) = -G_a(\tau, r)G_b(-\tau, r), \quad (50)$$

where a and b are the Fermi surface indices, r is an absolute value of a D -dimensional coordinate vector, τ is imaginary time. The vertex correction is neglected in Eq. (50). In Appendix A we show that the vertex correction to a linear response function does not affect the scaling properties. Using the long time and long distance asymptotics of the finite temperature Matsubara Green function which is given by Eq. (37), we find the asymptotics of the linear response functions:

$$\chi_{ab}(\tau, r) \propto \left| \frac{\pi T}{\sin(\pi T \tau)} \right|^{4h} \times \frac{\cos(k_+ r - \pi \frac{D-1}{2}) + \cos(k_- r)}{r^{2(D+1)h}}, \quad (51)$$

where $k_{\pm} = k_a \pm k_b$. The temporal part coincides with the SYK susceptibility, see Ref. [26]. The spatial part is dominated by the Kohn anomalies [47]. In case $a = b$ the Matsubara susceptibility $\chi_{aa}(\tau, r)$ has a non-oscillatory quasi-long-range component. The Fourier transform of Eq. (51) yields $\chi_{ab}(i\omega, q)$:

$$\chi_{ab}(i\omega, q) \propto \chi_M(i\omega) \chi_{ab}(q), \quad (52)$$

where

$$\chi_M(i\omega) = \frac{\Gamma(1-4h)}{\Lambda} \left| \frac{T}{\Lambda} \right|^{4h-1} \frac{\Gamma\left(2h + \frac{\omega}{2\pi T}\right)}{\Gamma\left(1-2h + \frac{\omega}{2\pi T}\right)} \quad (53)$$

and

$$\chi_{ab}(q \approx |k_{\pm}|) = \frac{(k_a k_b)^{D-(D+1)h} \Gamma\left(\frac{D+1}{2}(1-4h)\right)}{q^{\frac{D-1}{2}} |q - |k_{\pm}||^{\frac{D+1}{2}(1-4h)}} \times \cos\left(\frac{\pi}{4} [(D+1)(1-4h) \pm \text{sgn}(q - |k_{\pm}|)(D-1)]\right). \quad (54)$$

Here, the index M in $\chi_M(i\omega)$ stands for Matsubara susceptibility, and ω is the bosonic Matsubara frequency. We also restored the physical dimensions using Eq. (38), even though the overall numerical factor is suppressed. Equation (54) is also valid in the case $a = b$ with $k_- = 0$ where $\chi_{aa}(i\omega, q)$ is divergent for $q \rightarrow 0$. Analytically continuing $\chi_M(i\omega)$ to real frequencies we find the retarded linear response function:

$$\chi_R(\omega) = \frac{\Gamma(1-4h)}{\Lambda} \left| \frac{T}{\Lambda} \right|^{4h-1} \frac{\Gamma\left(2h - \frac{i\omega}{2\pi T}\right)}{\Gamma\left(1-2h - \frac{i\omega}{2\pi T}\right)}, \quad (55)$$

where ω is a real frequency. The imaginary part of the retarded linear response, describing the dissipation due to interaction effects, becomes:

$$\text{Im}(\chi_{ab}^R(\omega, q)) \propto \chi_{ab}(q) \text{Im}(\chi_R(\omega)), \quad (56)$$

$$\text{Im}(\chi_R(\omega)) = \cos(2\pi h) \frac{\Gamma(1-4h)}{\pi \Lambda} \left| \frac{T}{\Lambda} \right|^{4h-1} \times \sinh\left(\frac{\omega}{2T}\right) \left| \Gamma\left(2h + \frac{i\omega}{2\pi T}\right) \right|^2, \quad (57)$$

where $\chi_{ab}(q)$ is given by Eq. (54).

For $N = 2$ we have $h = 1/4$, which results in a divergence in Eq. (52). Regularizing this divergence, we find the retarded susceptibility for $h = 1/4$:

$$\chi_R(\omega) = \frac{1}{\Lambda} \left[\ln\left(\frac{\Lambda}{2\pi T}\right) - \psi\left(\frac{1}{2} - \frac{i\omega}{2\pi T}\right) \right], \quad h = \frac{1}{4}, \quad (58)$$

$$\text{Im}(\chi_R(\omega)) = \frac{\pi}{2\Lambda} \tanh\left(\frac{\omega}{2T}\right). \quad (59)$$

Here $\psi(z) = \Gamma'(z)/\Gamma(z)$ is the digamma function. The real part of $\chi_R(\omega)$ is logarithmically divergent at $\omega \gg T$. These equations correspond to the standard SYK susceptibility, see Ref. [26]. For $N = 2$ the Kohn anomalies are logarithmically divergent at $q \approx |k_{\pm}| = |k_a \pm k_b|$:

$$\chi_{ab}(q \approx |k_{\pm}|) \propto (k_a k_b)^{\frac{D}{2}} \left| \frac{k_a k_b}{q^2} \right|^{\frac{D-1}{4}} \ln \left| \frac{k_a k_b}{(q - |k_{\pm}|)^2} \right|. \quad (60)$$

From Eq. (60) we see that the susceptibility at $a = b$ and $q \rightarrow 0$ diverges as a power law with additional logarithmic divergence $\chi_{aa}(q \rightarrow 0) \rightarrow \ln(k_a/q)/q^{(D-1)/2}$.

The divergent Kohn anomalies given by Eq. (54) and the one-dimensional character of the radially nested scattering resonance may lead to spatially inhomogeneous orders. For example, coupling to intrinsic phonons can result in a charge density order due to the Peierls instability [48]. Another example comes from the Ruderman-Kittel-Kasuya-Yoshida (RKKY) exchange interaction between magnetic impurities which is mediated by itinerant fermions [49]. Magnetic helical order can be established if the spin susceptibility of the itinerant fermions has a divergent Kohn anomaly [50, 51].

Next, we derive the optical conductivity which takes the following form in the Matsubara representation [26, 52]:

$$\sigma_{\alpha\beta}(i\omega, q) = \frac{1}{\omega} \sum_{a, \mathbf{p}} T \sum_{\varepsilon} v_a^{\alpha} v_a^{\beta} G_a(i\varepsilon, \mathbf{p}) G_a(i(\varepsilon + \omega), \mathbf{p} + \mathbf{q}), \quad (61)$$

where we sum over the fermionic Matsubara frequencies ε and v_a^{α} is the α component of the current vertex. In Appendix A we argue that the current vertex renormalization does not affect the scaling in the conformal limit, i.e. we can use Eq. (61) with current vertices represented by the corresponding Fermi velocity v_a . Due to the separation of variables in the Green function, the ω -dependent part of the Matsubara optical conductivity is simply given by $\chi_M(i\omega)/\omega$, for $\chi_M(i\omega)$ see Eq. (53), while the q -dependent part is given by a power law because $G_a(i\omega, \delta p_a) \propto 1/|\delta p_a|^{1-2l}$, see Eq. (38). Analytically continuing to real frequencies, we find the retarded optical conductivity:

$$\sigma_{\alpha\beta}(\omega, q) = \delta_{\alpha\beta} \sigma(\omega, q), \quad \sigma(\omega, q) \propto \frac{\chi_R(\omega)}{i\omega} \frac{1}{q^{1-4l}}, \quad (62)$$

where $\delta_{\alpha\beta}$ appeared after the angular average over $v_a^{\alpha} v_a^{\beta}$, ω is a real frequency, and l is the spatial scaling dimension, see Eq. (25). We see from Eq. (62) that the dissipative real part of the optical conductivity is proportional to the imaginary part of the retarded susceptibility:

$$\text{Re}(\sigma(\omega, q)) \propto \frac{\text{Im}(\chi_R(\omega))}{\omega} \frac{1}{q^{1-4l}}. \quad (63)$$

In the limit $q \rightarrow 0$ the optical conductivity diverges due to the translational invariance in our system. The translational symmetry can be broken by either spatially

varying electric field that results in a finite q or by the finite size of the system (with open boundary conditions) which results in the infrared cut-off at $q \sim 1/L$, L is the system size. In this work we do not consider the effects of momentum non-conserving interactions like disorder or Umklapp scattering, i.e. we assume $L \ll \ell$, where ℓ is the mean free path. In such a clean limit $L \ll \ell$ the dc resistivity $\rho_{dc}(T, L)$ exhibits anomalous scaling with temperature and system size:

$$\rho_{dc}(T, L) = \frac{1}{\text{Re}(\sigma(\omega = 0, q = 1/L))} \propto \frac{T^{2-4h}}{L^{1-4l}}. \quad (64)$$

As $1 - 4l > 0$, the resistivity $\rho_{dc}(T, L)$ tends to zero for $L \rightarrow \infty$, as it should in absence of momentum non-conserving interactions. Thus, measuring the temperature and sample size dependence for $L \ll \ell$ of the static resistivity gives both the temporal h and spatial l conformal dimensions.

The case of $N = 2$ is particularly interesting. In this case, the dc resistivity is linear in temperature $\rho_{dc} \propto T$, see Eq. (64). This is the characteristic feature of strange metals which has been observed experimentally in cuprates [17, 18] and heavy fermion metals [19]. Current theories of strange metals [26–28] are based on the SYK model [24] that requires long-range interaction and random distribution of the interaction matrix elements. In our model the effective interaction is short range, see Eq. (5). Moreover, there is no randomness involved in the problem. Therefore, the new physical mechanism of the quantum criticality based on the resonant many-body exchange scattering that we propose in our study might play an important role in understanding the nature of strange metals.

VIII. CONCLUSIONS

In our study we theoretically discovered a novel physical state of strongly interacting fermions which can be realized in materials with multiple Fermi surfaces that are subject to a special resonant condition, FSR, given by Eq. (2). This phase can be experimentally identified by the spectral function showing no Landau quasiparticles close to the Fermi surface, by the anomalous power-law temperature and size dependence of the dc resistivity, and by the divergent susceptibilities in the static limit and at the Kohn anomalies. We believe that the new exotic phase that we predict in this work can be found, for instance, in semiconductor heterostructures because of the large interaction parameter $r_s \gg 1$. Moreover, the high quality and tunability of semiconductor devices makes it possible to tune the system to the FSR, see Eq. (2), which is required for establishing the new quantum critical state.

IX. ACKNOWLEDGEMENTS

We thank Oleg P. Sushkov for inspiring and stimulating discussions. We acknowledge support by the Georg H. Endress foundation, the Swiss National Science Foundation, and NCCR QSIT. This project received funding from the European Union’s Horizon 2020 research and innovation program (ERC Starting Grant, grant agreement No 757725).

Appendix A: LINEAR RESPONSE FUNCTIONS

In this section we make use of the conformal symmetry to demonstrate that the vertex corrections of the linear response functions, such as the dc conductivity and the charge susceptibilities, do not influence the critical exponents. We consider the general case of linear response function $\chi_{AB}(t, t')$, where A and B are some operators that are placed in the vertices of the response function. The dependence of χ_{AB} on the effective spatial coordinates x, x' can be considered analogously. Here we use the relation between the linear response functions and the four-point Green function $G^{(4)}(t_1, t_2; t_3, t_4)$:

$$\chi_{AB}(t, t') = \text{Tr} \left(A G^{(4)}(t, t; t', t') B \right), \quad (A1)$$

where Tr stands for the trace over the index space. It is not important for us how exactly the trace is taken, here we are after the time scaling of $\chi_{AB}(t, t')$. The global conformal symmetry (it consists of the translations, dilatations, and special conformal transformations) restricts the four-point Green function to the following form [53]:

$$G^{(4)}(t_1, t_2; t_3, t_4) = F(\tau) \prod_{i < j} t_{ij}^{-\frac{2h}{3}}, \quad \tau = \frac{t_{13}t_{24}}{t_{14}t_{23}}, \quad (A2)$$

where $t_{ij} = t_i - t_j$, τ is the conformal cross-ratio, $F(\tau)$ is some function of the cross-ratio, h is the temporal conformal dimension, see Eq. (25). Equation (A2) explicitly separates the pairwise singularities when $t_i \rightarrow t_j$. The scaling of t_{ij} can be found from applying the rescaling of times $t_i \rightarrow st_i$. On the one hand, each of the four fields in $G^{(4)}$ has conformal dimension h , so $G^{(4)}$ acquires the factor s^{-4h} . On the other hand, the factor s comes from each of the six t_{ij} which fixes their power to $-2h/3$. In order to calculate $\chi_{AB}(t, t')$, we have to put $t_1 = t_2 = t$, $t_3 = t_4 = t'$, see Eq. (A1). This leads to singularities in Eq. (A2) since $t_{12} = t_{34} = 0$. This problem can be avoided by setting small non-zero t_{12} and t_{34} and express them in terms of non-zero $t_{13} = t_{14} = t_{23} = t_{24} = t - t'$:

$$t_{12}t_{34} = \frac{\tau - 1}{\tau} t_{13}t_{24} = \frac{\tau - 1}{\tau} (t - t')^2. \quad (A3)$$

Then we substitute it in Eq. (A2) and take the limit $t_{12} \rightarrow 0$, $t_{34} \rightarrow 0$ which is after all equivalent to the limit

$\tau \rightarrow 1$:

$$G^{(4)}(t, t; t', t') = \lim_{\tau \rightarrow 1} \left(F(\tau) \left(\frac{\tau - 1}{\tau} \right)^{-\frac{2h}{3}} \right) (t - t')^{-4h}. \quad (\text{A4})$$

The limit at $\tau = 1$ yields some constant that we are not interested in. An important consequence of Eq. (A4) is the universal scaling of the linear response function with time, $\chi_{AB}(t, t') \propto |t - t'|^{-4h}$. The dependence of the linear response function on the effective radial coordinate can be deduced similarly. So, the conformal symmetry allows us to restore the time and coordinate scaling of any linear response function at zero temperature $T = 0$:

$$\chi_{AB}(t, x, t', x') \propto |x - x'|^{-4l} |t - t'|^{-4h}, \quad (\text{A5})$$

where l and h are the spatial and the temporal conformal dimensions, respectively, see Eq. (25). Note that this scaling is entirely determined by the conformal symmetry. In particular, $\chi_{AB}(t, x, t', x')$ contains all corrections to the linear response vertex.

It is worth mentioning that the linear response function with all vertex corrections neglected has exactly the same scaling:

$$\begin{aligned} \chi_{AB}^{(0)}(t, x, t', x') &= \text{Tr} (G(t - t', x - x') A G(t' - t, x' - x) B) \\ &\propto |x - x'|^{-4l} |t - t'|^{-4h}. \end{aligned} \quad (\text{A6})$$

In this case the scaling is given directly by the two-point Green function, see Eqs. (26), (34), and (35). This allows us to conclude that the corrections to the linear response

vertices do not influence the time and coordinate scaling of the linear response function. The vertex correction is also not important at finite temperature T because it corresponds to a certain conformal transformation, see Ref. [25].

Appendix B: COMMENTS ON THE ONE-DIMENSIONAL CASE

All the results that we provide in the main text are only valid for $D > 1$ due to the separation of temporal and spatial dynamics, see Eq. (26). In case of $D = 1$ one has to figure out appropriate linear combinations of x and τ . Usually, these combinations correspond to the left and right movers in real time and to complex coordinates $x \pm i\tau$ in the imaginary time [53].

In the truly one-dimensional case one has to bosonize the effective interaction $V(R)$ given by Eq. (5). We recall that $V(R)$ contains C_{2N}^N different terms half of which are conjugates. Right at the FSR that is given by Eq. (2) $V(R)$ contains slowly varying terms that can be combined into C_{2N}^N non-commuting cosines. At this point it is not exactly clear how to proceed with such a large number of non-commuting interaction terms. However, due to the competing nature of these cosines we also expect a highly non-trivial quantum critical phase in this case. The case of two non-commuting cosines corresponds to the self-dual sine Gordon model that describes parafermions [54]. Exactly solvable extensions of the sine Gordon model are typically built via extending the underlying symmetry group [39, 55].

-
- [1] N. W. Ashcroft and N. D. Mermin, *Solid State Physics* (Saunders College, Philadelphia, 1976).
- [2] E. Fermi, *Zur Quantelung des Idealen Einatomigen Gases*, Z. Phys. **36**, 902 (1926).
- [3] S.-i. Tomonaga, *Remarks on Bloch's Method of Sound Waves Applied to Many-Fermion Problems*, Prog. Theor. Phys. **5**, 544-569 (1950).
- [4] J. M. Luttinger, *An Exactly Soluble Model of a Many-Fermion System*, J. Math. Phys. **4**, 1154 (1963).
- [5] D. C. Mattis and E. H. Lieb, *Exact Solution of a Many-Fermion System and its Associated Boson Field*, J. Math. Phys. **6**, 304 (1965).
- [6] L. D. Landau, *The Theory of a Fermi Liquid*, Sov. Phys. JETP **3**, 920 (1957).
- [7] K. Seo, V. N. Kotov, and B. Uchoa, *Ferromagnetic Mott State in Twisted Graphene Bilayers at the Magic Angle*, Phys. Rev. Lett. **122**, 246402 (2019).
- [8] Y. Jiang, X. Lai, K. Watanabe, T. Taniguchi, K. Haule, J. Mao, and E. Y. Andrei, *Charge Order and Broken Rotational Symmetry in Magic-Angle Twisted Bilayer Graphene*, Nature **573**, 91–95 (2019).
- [9] Y. Cao, V. Fatemi, S. Fang, K. Watanabe, T. Taniguchi, E. Kaxiras, and P. Jarillo-Herrero, *Unconventional Superconductivity in Magic-Angle Graphene Superlattices*, Nature **556**, 43–50 (2018).
- [10] T. Ando, A. B. Fowler, and F. Stern, *Electronic Properties of Two-Dimensional Systems*, Rev. Mod. Phys. **54**, 437 (1982).
- [11] G. Scappucci, C. Kloeffer, F. A. Zwanenburg, D. Loss, M. Myronov, J.-J. Zhang, S. De Franceschi, G. Katsaros, and M. Veldhorst, *The Germanium Quantum Information Route*, arXiv:2004.08133.
- [12] W. Heisenberg, *Mehrkörperproblem und Resonanz in der Quantenmechanik*, Z. Phys. **38**, 411–426 (1926).
- [13] E. Fradkin, *Field Theories of Condensed Matter Physics* (Cambridge University Press, ed. 2, 2013).
- [14] L. D. Landau and I. Y. Pomeranchuk, *On the Properties of Metals at Very Low Temperatures*, Sov. Phys. JETP, **7**, 379 (1937).
- [15] S. Sachdev, *Quantum Phase Transitions* (Cambridge University Press, ed. 2, 2011).
- [16] P. Coleman and A. J. Schofield, *Quantum criticality*, Nature **433**, 226–229 (2005).
- [17] R. Daou, N. Doiron-Leyraud, D. LeBoeuf, S. Y. Li, F. Laliberté, O. Cyr-Choinière, Y. J. Jo, L. Balicas, J.-Q. Yan, J.-S. Zhou, J. B. Goodenough, and L. Taillefer, *Linear Temperature Dependence of Resistivity and Change in the Fermi Surface at the Pseudogap Critical Point of*

- a High- T_c Superconductor*, Nat. Phys. **5**, 31–34 (2009).
- [18] B. Keimer, S. A. Kivelson, M. R. Norman, S. Uchida, and J. Zaanen, *From Quantum Matter to High-Temperature Superconductivity in Copper Oxides*, Nature **518**, 179–186 (2015).
- [19] P. Gegenwart, Q. Si, and F. Steglich, *Quantum Criticality in Heavy-Fermion Metals*, Nat. Phys. **4**, 186–197 (2008).
- [20] A. V. Chubukov, S. Sachdev, and J. Ye, *Theory of Two-Dimensional Quantum Heisenberg Antiferromagnets with a Nearly Critical Ground State*, Phys. Rev. B **49**, 11919 (1994).
- [21] A. Abanov, A. V. Chubukov, and J. Schmalian, *Quantum-Critical Theory of the Spin-Fermion Model and its Application to Cuprates: Normal State Analysis*, Adv. Phys. **52**(3), 119–218 (2003).
- [22] H. v. Löhneysen, A. Rosch, M. Vojta, and P. Wölfle, *Fermi-Liquid Instabilities at Magnetic Quantum Phase Transitions*, Rev. Mod. Phys. **79**, 1015 (2007).
- [23] T. Senthil, *Critical Fermi Surfaces and Non-Fermi Liquid Metals*, Phys. Rev. B **78**, 035103 (2008).
- [24] S. Sachdev and J. Ye, *Gapless Spin-Fluid Ground State in a Random Quantum Heisenberg Magnet*, Phys. Rev. Lett. **70**, 3339 (1993).
- [25] S. Sachdev, *Bekenstein-Hawking Entropy and Strange Metals*, Phys. Rev. X **5**, 041025 (2015).
- [26] O. Parcollet and A. Georges, *Non-Fermi-Liquid Regime of a Doped Mott Insulator*, Phys. Rev. B **59**, 5341 (1999).
- [27] D. Chowdhury, Y. Werman, E. Berg, and T. Senthil, *Translationally Invariant Non-Fermi-Liquid Metals with Critical Fermi Surfaces: Solvable Models*, Phys. Rev. X **8**, 031024 (2018).
- [28] R. A. Davison, K. Schalm, and J. Zaanen, *Holographic Duality and the Resistivity of Strange Metals*, Phys. Rev. B **89**, 245116 (2014).
- [29] M. Dresselhaus, G. Dresselhaus, S. B. Cronin, and A. G. S. Filho, *Solid State Properties: From Bulk to Nano* (Springer, Berlin, Heidelberg, ed. 1, 2018).
- [30] A. Manchon, H. C. Koo, J. Nitta, S. M. Frolov, and R. A. Duine, *New Perspectives for Rashba Spin-Orbit Coupling*, Nat. Mater. **14**, 871–882 (2015).
- [31] F. Dettwiller, J. Fu, S. Mack, P. J. Weigele, J. C. Egues, D. D. Awschalom, and D. M. Zumbühl, *Stretchable Persistent Spin Helices in GaAs Quantum Wells*, Phys. Rev. X **7**, 031010 (2017).
- [32] A. Kriisa, R. L. Samaraweera, M. S. Heimbeck, H. O. Everitt, C. Reichl, W. Wegscheider, and R. G. Mani, *Cyclotron Resonance in the High Mobility GaAs/AlGaAs 2D Electron System Over the Microwave, mm-wave, and Terahertz- Bands*, Sci. Rep. **9**, 2409 (2019).
- [33] M.-H. Whangbo, E. Canadell, P. Foury, and J.-P. Pouget, *Hidden Fermi Surface Nesting and Charge Density Wave Instability in Low-Dimensional Metals*, Science **252**, 96–98 (1991).
- [34] S. Murayama, C. Sekine, A. Yokoyanagi, K. Hoshi, and Y. Ōnuki, *Uniaxial Fermi-Surface Nesting and Spin-Density-Wave Transition in the Heavy-Fermion Compound $Ce(Ru_{0.85}Rh_{0.15})_2Si_2$* , Phys. Rev. B **56**, 11092 (1997).
- [35] L. Trifunovic, D. Loss, and J. Klinovaja, *From Coupled Rashba Electron- and Hole-Gas Layers to Three-Dimensional Topological Insulators*, Phys. Rev. B **93**, 205406 (2016).
- [36] Y. Volpez, D. Loss, and J. Klinovaja, *Three-Dimensional Fractional Topological Insulators in Coupled Rashba Layers*, Phys. Rev. B **96**, 085422 (2017).
- [37] A. R. Hamilton, E. H. Linfield, M. J. Kelly, D. A. Ritchie, G. A. C. Jones, and M. Pepper, *Transition from One- to Two-Subband Occupancy in the 2DEG of Back-Gated Modulation-Doped $GaAs-Al_xGa_{1-x}As$ Heterostructures*, Phys. Rev. B **51**, 17600 (1995).
- [38] Z. W. Zheng, B. Shen, R. Zhang, Y. S. Gui, C. P. Jiang, Z. X. Ma, G. Z. Zheng, S. L. Guo, Y. Shi, P. Han, Y. D. Zheng, T. Someya, and Y. Arakawa, *Occupation of the Double Subbands by the Two-Dimensional Electron Gas in the Triangular Quantum Well at $Al_xGa_{1-x}N/GaN$ Heterostructures*, Phys. Rev. B **62**, R7739(R) (2000).
- [39] J. C. Y. Teo and C. L. Kane, *From Luttinger Liquid to Non-Abelian Quantum Hall States*, Phys. Rev. B **89**, 085101 (2014).
- [40] J. Klinovaja and Y. Tserkovnyak, *Quantum Spin Hall Effect in Strip of Stripes Model*, Phys. Rev. B **90**, 115426 (2014).
- [41] P. P. Aseev, D. Loss, and J. Klinovaja, *Conductance of Fractional Luttinger Liquids at Finite Temperatures*, Phys. Rev. B **98**, 045416 (2018).
- [42] H. Lehmann, *Über Eigenschaften von Ausbreitungsfunktionen und Renormierungskonstanten Quantisierter Felder*, Nuovo Cim. **11**, 342–357 (1954).
- [43] I. Y. Pomeranchuk, *On the Stability of a Fermi Liquid*, Sov. Phys. JETP **8**, 361 (1958).
- [44] R. Gurau, *Notes on Tensor Models and Tensor Field Theories*, arXiv:1907.03531v2.
- [45] J. Maldacena, *The Large- N Limit of Superconformal Field Theories and Supergravity*, Int. J. Theor. Phys. **38**, 1113–1133 (1999).
- [46] P. Stano, J. Klinovaja, A. Yacoby, and D. Loss, *Local Spin Susceptibilities of Low-Dimensional Electron Systems*, Phys. Rev. B **88**, 045441 (2013).
- [47] W. Kohn, *Image of the Fermi Surface in the Vibration Spectrum of a Metal*, Phys. Rev. Lett. **2**, 393 (1959).
- [48] R. E. Peierls, *Quantum Theory of Solids* (Clarendon, Oxford, 1955).
- [49] M. A. Ruderman and C. Kittel, *Indirect Exchange Coupling of Nuclear Magnetic Moments by Conduction Electrons*, Phys. Rev. **96**, 99 (1954).
- [50] B. Braunecker, P. Simon, and D. Loss, *Nuclear Magnetism and Electron Order in Interacting One-Dimensional Conductors*, Phys. Rev. B **80**, 165119 (2009).
- [51] C. P. Scheller, T.-M. Liu, G. Barak, A. Yacoby, L. N. Pfeiffer, K. W. West, and D. M. Zumbühl, *Possible Evidence for Helical Nuclear Spin Order in GaAs Quantum Wires*, Phys. Rev. Lett. **112**, 066801 (2014).
- [52] A. Georges, G. Kotliar, W. Krauth, and M. J. Rozenberg, *Dynamical Mean-Field Theory of Strongly Correlated Fermion Systems and the Limit of Infinite Dimensions*, Rev. Mod. Phys. **68**, 13 (1996).
- [53] P. H. Ginsparg, *Applied Conformal Field Theory*, arXiv:9108028v1.
- [54] P. Lecheminant, A. O. Gogolin, and A. A. Nersisyan, *Criticality in Self-Dual Sine-Gordon Models*, Nucl. Phys. B **639**(3), 502–523 (2002).
- [55] I. I. Kogan, B. Tekin, and A. Kovner, *Deconfinement at $N > 2$: $SU(N)$ Georgi-Glashow Model in 2+1 Dimensions*, J. High Energy Phys. **2001**(05), 062 (2001).